

**Beam-splitter switches based on zenithal bistable liquid-crystal gratings**Dimitrios C. Zografopoulos<sup>\*</sup> and Romeo Beccherelli<sup>†</sup>*Consiglio Nazionale delle Ricerche, Istituto per la Microelettronica e Microsistemi, Via del Fosso del Cavaliere 100, 00133 Rome, Italy*Emmanouil E. Kriezis<sup>‡</sup>*Department of Electrical and Computer Engineering, Aristotle University of Thessaloniki, Thessaloniki GR-54124, Greece*

(Received 9 August 2014; published 17 October 2014)

The tunable optical diffractive properties of zenithal bistable nematic liquid-crystal gratings are theoretically investigated. The liquid-crystal orientation is rigorously solved via a tensorial formulation of the Landau–de Gennes theory and the optical transmission properties of the gratings are investigated via full-wave finite-element frequency-domain simulations. It is demonstrated that by proper design the two stable states of the grating can provide nondiffracting and diffracting operation, the latter with equal power splitting among different diffraction orders. An electro-optic switching mechanism, based on dual-frequency nematic materials, and its temporal dynamics are further discussed. Such gratings provide a solution towards tunable beam-steering and beam-splitting components with extremely low power consumption.

DOI: [10.1103/PhysRevE.90.042503](https://doi.org/10.1103/PhysRevE.90.042503)

PACS number(s): 61.30.Jf, 42.79.Kr, 42.79.Dj, 42.70.Df

**I. INTRODUCTION**

Nematic liquid crystals (LCs) are inherently anisotropic organic materials whose orientation can be dynamically controlled via the application of external electric, magnetic, or optical fields. They have been under intense investigation as the key element for addressable devices in a broad range of applications spanning from displays to tunable filters, waveguides, beam steerers, and spatial light modulators for photonics in the visible (VIS) or infrared (IR) spectrum [1–8]. The properties of LC-based devices are directly associated with the nematic molecular orientation in space, which in turn depends on the geometry, anchoring conditions at the surfaces of the LC cavity, and the applied stimuli, e.g., a low-frequency electric field that actuates the LC molecules in the case of electro-optic components. The dynamical tuning of the device properties is performed by adjusting the amplitude and direction of the electric field, typically applied via transparent electrodes such as indium-tin-oxide (ITO) thin films in the VIS or IR. Thus, continuous tuning or switching can be achieved between the off-field equilibrium state, which minimizes the total energy in the LC volume, and the on-field states that depend on the applied voltage.

In a different approach, it has been demonstrated that certain LC geometries that involve periodical grating structures in one or two dimensions can be bistable, meaning that there are two equilibrium stable states corresponding to different molecular orientation profiles [9–21]. Such geometries allow for the design of devices with zero power consumption, except when switching between the two states is required. This concept has been exploited in the development of passively addressed displays for image storing, based on the zenithal bistable (ZB) device, one of the most extensively investigated LC bistable structures [9,11–14,18,19]. In this configuration, the LC is confined in a cell formed between a flat top surface

and a bottom grating structure, both of which are typically treated so as to provide homeotropic (perpendicular) molecular alignment. By proper design, the device can appear dark or bright when viewed between crossed polarizers with high contrast values provided by the two LC states. Moreover, the surface-induced bistability provides a series of favorable features, such as high tolerance to mechanical stress and no image sticking [22].

Although much effort has been devoted to the design of LC zenithal bistable structures for display applications, they have been almost unexplored when it comes to the potential of tuning their optical properties [23]. In this work, we demonstrate switchable beam splitting in ZB optical diffraction gratings (DGs). Liquid-crystal tunable diffractive gratings have been thus far demonstrated using different tuning mechanisms, such as the electro-optical effect [24–28], tunable photoalignment [29–31], and all-optical switching via the illumination of azo-dye LC mixtures [32–34]. The proposed LC-ZB-DG relies on the electro-optic switching mechanism, thus resulting in zero idle and very low switching power consumption, as well as fast switching speeds. Compared to typical electro-optically controlled LC gratings, which demand constant power consumption to keep the grating in the switched state, these LC-ZB-DGs may allow for orders of magnitude longer operation times, depending on the duty cycle of the device. Furthermore, it eliminates the need for external optical sources or masks, which cannot be easily integrated, such as those used in light-induced azo-dye or photoalignment-based switching. By proper selection of the material and geometrical parameters in sinusoidal and triangular LC-ZB-DGs, tunable optical power beam splitting is demonstrated by switching between the two stable LC states. The LC orientation problem is rigorously solved by employing a tensorial formulation [35] capable of capturing the defect singularities and nematic order parameter variations in ZB structures, whereas the optical diffraction properties are calculated via full-wave finite-element simulations [36]. In addition, a switching configuration is investigated based on the use of dual-frequency LC materials and its temporal dynamics are resolved, showing that the optical response

<sup>\*</sup>Corresponding author: [dimitrios.zografopoulos@artov.imm.cnr.it](mailto:dimitrios.zografopoulos@artov.imm.cnr.it)<sup>†</sup>[romeo.beccherelli@artov.imm.cnr.it](mailto:romeo.beccherelli@artov.imm.cnr.it)<sup>‡</sup>[mkriezis@auth.gr](mailto:mkriezis@auth.gr)

of the device is faster than the LC relaxation dynamics. The proposed elements may find applications as ultralow-power components in consumer electronics devices, such as holographic switches, projection systems, or CD or DVD systems.

## II. ZENITHAL BISTABLE LIQUID-CRYSTAL DIFFRACTION GRATINGS AS TUNABLE OPTICAL BEAM SPLITTERS

### A. Liquid-crystal orientation studies in zenithal bistable gratings

The study of liquid-crystal orientation in confined geometries involves the minimization of the LC free energy, which is associated with surface and bulk deformations, the LC thermodynamical equilibrium, and any external applied electric fields. In the case of ZB structures, it has been shown that the two stable states correspond to a high-tilt, vertical aligned nematic (VAN), and a low-tilt, hybrid aligned nematic (HAN) configuration [9,12,14,19]. The latter is characterized by the presence of two point defects, which lead to point singularities when the LC problem is treated by the classical Frank continuum model that represents the nematic director via a unit vector whose spatial variations describe the LC distortions. Thus, in this work we employ the  $\mathbf{Q}$  tensor formalism, which allows for biaxial solutions, nematic order variations, and the resolution of defects, and avoids the use of Euler angles for the description of the nematic orientation. The free LC energy is expanded in terms described by the elements  $q_i$  of the symmetric traceless matrix

$$\mathbf{Q} = \begin{pmatrix} q_1 & q_2 & q_3 \\ q_2 & q_4 & q_5 \\ q_3 & q_5 & -q_1 - q_4 \end{pmatrix}, \quad (1)$$

and their spatial derivatives  $\nabla q_i$ . In the most general case of biaxial configurations the  $\mathbf{Q}$  matrix, also termed as the tensor order parameter, can be expressed as

$$\mathbf{Q} = S_1(\mathbf{n} \otimes \mathbf{n}) + S_2(\mathbf{m} \otimes \mathbf{m}) - \frac{1}{3}(S_1 + S_2)\mathbf{I}, \quad (2)$$

where  $\mathbf{I}$  is the identity matrix and  $\mathbf{n}$ ,  $\mathbf{m}$ , and  $\mathbf{n} \times \mathbf{m}$  are its eigenvectors with corresponding eigenvalues  $(2S_1 - S_2)/3$ ,  $(2S_2 - S_1)/3$ , and  $-(S_1 + S_2)/3$ . Purely uniaxial solutions exist when two eigenvalues are equal leading to  $\mathbf{Q} = S[(\mathbf{n} \otimes \mathbf{n}) - (1/3)\mathbf{I}]$ .

The free energy  $F$  in the LC bulk is given by

$$F = \iiint_V F_b dV = \iiint_V (F_{\text{th}} + F_{\text{el}} + F_{\text{em}}) dV, \quad (3)$$

where  $F_b$  is the total energy density function and  $F_{\text{th}}$ ,  $F_{\text{el}}$ , and  $F_{\text{em}}$  describe the thermotropic, elastic, and electromagnetic contributions, respectively. We have not included a surface term in Eq. (3), as we assume strong homeotropic anchoring at the LC/polymer interfaces. This is mathematically equivalent to the Dirichlet condition  $\mathbf{Q} = \mathbf{Q}_s$ , where  $\mathbf{Q}_s$  is the prescribed order tensor at the boundary. In the case here considered this is given by  $q_{1s} = v_x^2 - 1/3$ ,  $q_{2s} = v_x v_y$ ,  $q_{3s} = v_x v_z$ ,  $q_{4s} = v_y^2 - 1/3$ ,  $q_{5s} = v_y v_z$ , where  $v_j$  are the components of the unit vector  $\mathbf{v}$  perpendicular to the surface. Homeotropic alignment can be achieved by coating

the surfaces with a thin, even monomolecular, layer of an appropriate surfactant material [12,37].

The thermotropic energy  $F_{\text{th}}$  is expressed via a Taylor expansion around  $\mathbf{Q} = \mathbf{0}$ :

$$F_{\text{th}} = a \text{tr}(\mathbf{Q}^2) + \frac{2b}{3} \text{tr}(\mathbf{Q}^3) + \frac{c}{2} [\text{tr}(\mathbf{Q}^2)]^2, \quad (4)$$

where  $\text{tr}(\cdot)$  denotes the trace of a matrix and the thermotropic coefficients are equal to  $a = -0.3 \times 10^5 \text{ J/m}^3$ ,  $b = -1.5 \times 10^5 \text{ J/m}^3$ , and  $c = 2.5 \times 10^5 \text{ J/m}^3$  [38,39]. These values lead to an equilibrium order parameter equal to  $S_{\text{eq}} = 0.6$ , which is typical of LC materials in the nematic state. The elastic energy, which originates from the distortion of the nematic molecules in space, is described by

$$F_{\text{el}} = \sum_{i,j,k=1,2,3} \left[ \frac{L_1}{2} \left( \frac{\partial Q_{ij}}{\partial x_k} \right)^2 + \frac{L_2}{2} \frac{\partial Q_{ij}}{\partial x_j} \frac{\partial Q_{ik}}{\partial x_k} \right] + \sum_{i,j,k,l=1,2,3} \left[ \frac{L_6}{2} Q_{lk} \frac{\partial Q_{ij}}{\partial x_l} \frac{\partial Q_{ij}}{\partial x_k} \right]. \quad (5)$$

The elastic parameters  $L_i$  are related to the Frank elastic constants  $K_{ii}$  via the expressions  $L_1 = (K_{33} - K_{11} + 3K_{22})/(6S_{\text{exp}}^2)$ ,  $L_2 = (K_{11} - K_{22})/S_{\text{exp}}^2$ , and  $L_6 = (K_{33} - K_{11})/(2S_{\text{exp}}^3)$ . In this work, we consider the commercial mixture E7 as the nematic material, which is characterized by  $K_{11} = 10.3 \text{ pN}$ ,  $K_{22} = 7.4 \text{ pN}$ , and  $K_{33} = 16.48 \text{ pN}$  [40]. In addition, we assume that the experimental nematic order parameter  $S_{\text{exp}}$ , i.e., when the elastic constants were measured, is equal to  $S_{\text{eq}} = 0.6$ .

The electrostatic energy in the presence of an external electric field is given by

$$F_{\text{em}} = - \int \mathbf{D} \cdot d\mathbf{E}, \quad (6)$$

where  $\mathbf{D}$  is the displacement field and  $\mathbf{E}$  the electric field. The displacement field is given by the constitutive equation

$$\mathbf{D} = \varepsilon_0 \tilde{\varepsilon}_r \mathbf{E} + \mathbf{P}_s, \quad (7)$$

where  $\varepsilon_0$  is vacuum permittivity,  $\tilde{\varepsilon}_r$  is the LC dielectric tensor, and  $\mathbf{P}_s$  is the spontaneous polarization vector. For nematic materials the dielectric tensor is given by

$$\tilde{\varepsilon}_r = \Delta \varepsilon^* \mathbf{Q} + \bar{\varepsilon} \mathbf{I}, \quad (8)$$

where  $\Delta \varepsilon^* = (\varepsilon_{\parallel} - \varepsilon_{\perp})/S_{\text{exp}}$  is the scaled dielectric anisotropy and  $\bar{\varepsilon} = (\varepsilon_{\parallel} + 2\varepsilon_{\perp})/3$ . In the case of E7, the relative LC permittivities are equal to  $\varepsilon_{\parallel} = 18.6$  and  $\varepsilon_{\perp} = 5.31$  [40].

The spontaneous polarization derives from the flexoelectric effect, which is owing to shape asymmetry of the LC molecules or distortion of molecular pairwise coupling. The  $i$ th component of the flexoelectric polarization is given by

$$P_i = p_1 \sum_{j=1,2,3} \frac{\partial Q_{ij}}{\partial x_j} + p_2 \sum_{j,k=1,2,3} Q_{ij} \frac{\partial Q_{jk}}{\partial x_k}, \quad (9)$$

where  $p_1 = (e_{11} + e_{33})/(2S_{\text{exp}})$  and  $p_2 = (e_{11} - e_{33})/(2S_{\text{exp}}^2)$  are terms depending on the classical flexoelectric polarization coefficients  $e_{11}$  and  $e_{33}$ , as these appear in

$$\mathbf{P}_s = e_{11}(\nabla \cdot \mathbf{n})\mathbf{n} + e_{33}(\nabla \times \mathbf{n}) \times \mathbf{n}, \quad (10)$$

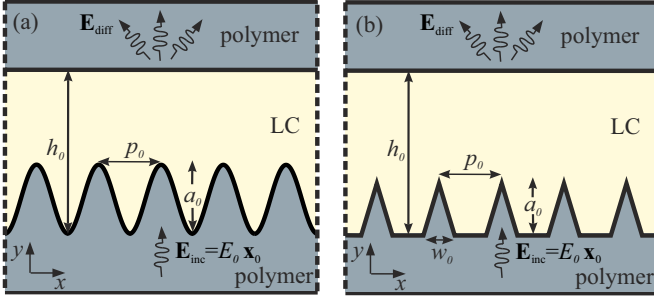


FIG. 1. (Color online) Schematic layout and parameter definition of the two proposed zenithal bistable liquid-crystal diffraction gratings: (a) sinusoidal and (b) triangular. The incident field is an  $x$ -polarized plane wave impinging normally from the substrate side.

where  $\mathbf{n}$  is the nematic director [39]. It is stressed that Eq. (10) is not directly comparable to (9), since it cannot account for variations of the nematic order parameter. Here, we consider the values  $e_{11} + e_{33} = 15$  pC/m and  $e_{11} - e_{33} = 10$  pC/m for E7 [41].

The free energy  $F$  can be minimized via the solution of the set of five Euler-Lagrange equations given by

$$\sum_{j=1}^3 \frac{\partial}{\partial x_j} \left( \frac{\partial F_b}{\partial q_{i,j}} \right) - \frac{\partial F_b}{\partial q_i} = \gamma_1^* \frac{\partial D}{\partial \dot{q}_i}, \quad (11)$$

for  $i = 1 \dots 5$ , where  $q_{i,j} = \partial q_i / \partial x_j$ ,  $x_j$  being the unit vectors of the three-dimensional Cartesian system. The right-hand side of (11) describes the dynamic evolution of the  $\mathbf{Q}$  tensor via the dissipation function  $D = \text{tr}(\dot{\mathbf{Q}}^2)$ , where  $\dot{\mathbf{Q}} = \partial \mathbf{Q} / \partial t$ . The term  $\gamma_1^*$  is related to the LC rotational viscosity  $\gamma_1$  via  $\gamma_1^* = \gamma_1 / (4S_{\text{exp}}^2)$  [20], equal to 282.8 mPa s for E7 [42].

The geometry of the LC-ZB gratings under investigation is depicted in Fig. 1. We consider two cases: sinusoidal and triangular gratings, both of which have been shown to support the VAN and HAN states [12,19]. The grating and the superstratum are made of a polymer material. The grating pitch is  $p_0$  and its amplitude  $a_0$ , while the LC cell thickness is fixed at  $h_0 = 10 \mu\text{m}$ . In the case of triangular gratings, another degree of freedom is introduced, the width of the triangular element base, which is  $w_0 = fp_0$ ,  $f$  being a filling factor. The set of Euler-Lagrange equations (11) is solved in a unit cell of the LC region, assuming strong homeotropic anchoring on the top and bottom surfaces and periodic boundary conditions laterally. Figure 2 shows the nematic director profiles and the spatial distribution of the  $q_1$  element of the tensor order parameter for a sinusoidal grating with  $p_0 = 2.5 \mu\text{m}$  and  $a_0 = 4 \mu\text{m}$ . In the VAN state the LC molecules are mostly aligned perpendicular to the substrate and no defects are observed. On the contrary, in the HAN state two defects of opposite topological charge  $\pm \frac{1}{2}$  appear at the peak and the trough of the grating. The molecular orientation is mostly parallel to the substrate in the vicinity of the grating and progressively rotates in order to assume perpendicular anchoring at the top surface.

The bistable states of the triangular grating are investigated in Fig. 3 for  $p_0 = 2.5 \mu\text{m}$ ,  $a_0 = 4 \mu\text{m}$ , and  $f = 0.5$ . As in the case of the sinusoidal grating, the VAN state exhibits mainly perpendicular molecular alignment, except for the regions close to the grating walls where the molecules are anchored.

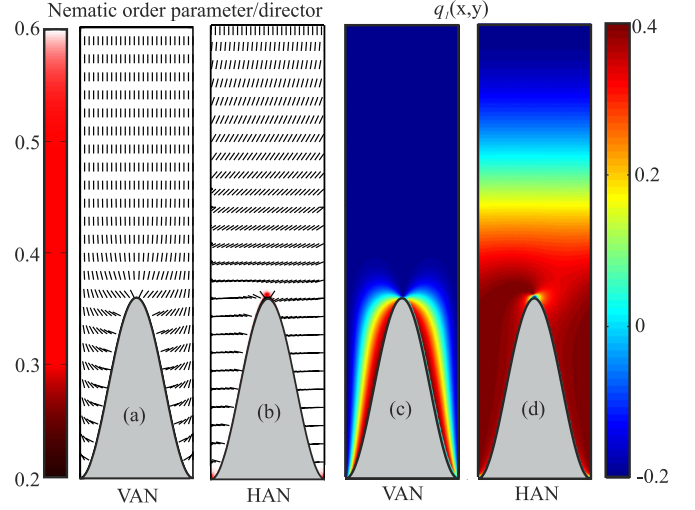


FIG. 2. (Color online) Nematic director and the  $q_1$  tensor element profiles for the VAN [(a), (c)] and HAN [(b), (d)] states of the sinusoidal grating, for  $p_0 = 2.5 \mu\text{m}$  and  $a_0 = 4 \mu\text{m}$ . The background in (a) and (b) shows the profile of the nematic order parameter, where reddish spots correspond to lower values and indicate the presence of defects. Two defects of opposite topological strength are formed in the HAN state at the peak and trough of the grating. Large values of  $q_1$  indicate molecular alignment along the  $x$  axis.

However, owing to the different geometry, point defects are observed at the base and the peak of the triangular elements. In the HAN state, a pair of point defects is also observed, at the base of the elements. The LC molecules are parallel to the  $x$  axis around the grating, except for a small region on the flat surface that connects the base of the triangular elements. The reduction of  $w_0$  with respect to the grating pitch

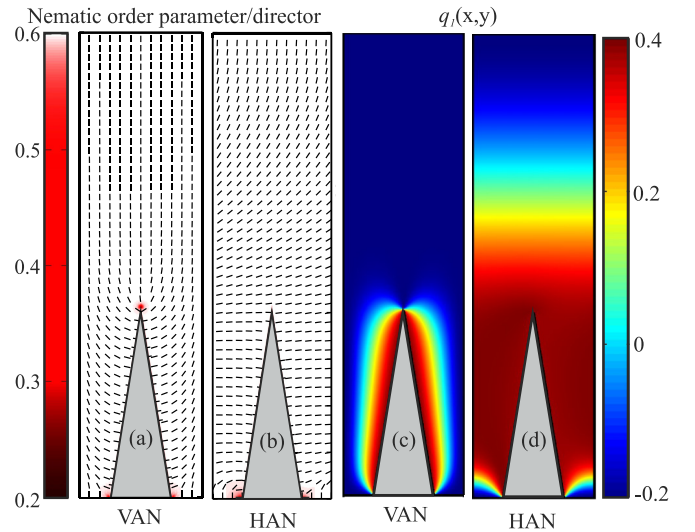


FIG. 3. (Color online) Nematic director, order parameter, and the  $q_1$  tensor element profiles for the VAN [(a), (c)] and HAN [(b), (d)] states of the triangular grating, where  $p_0 = 2.5 \mu\text{m}$ ,  $a_0 = 4 \mu\text{m}$ , and  $f = w_0/p_0 = 0.5$ . Contrary to the sinusoidal grating of Fig. 2, the two defects of opposite topological strength observed in the HAN state are located at the base of the triangular grating elements.

and the difference in the element shape is the reason for the dissimilarities observed between the sinusoidal and triangular gratings. Nevertheless, the overall molecular alignment shares the same features for both the sinusoidal and the triangular geometry.

### B. Optical diffractive properties of liquid-crystal zenithal bistable gratings

The LC molecular orientation for the two stable states of the gratings affects directly their optical diffractive properties, as it creates a region of varying refractive index in the vicinity of the grating. The LC optical properties are described by the tensor of (8), where the LC permittivities now refer to the optical frequencies, namely  $\varepsilon_{\parallel} = n_e^2$  and  $\varepsilon_{\perp} = n_o^2$ , with  $n_e$  and  $n_o$  being the LC extraordinary and ordinary refractive indices, respectively. These are equal to  $n_o = 1.519$  and  $n_e = 1.73$  for E7 at the free-space wavelength  $\lambda = 633$  nm [43], which is the target wavelength of operation. The design procedure described in this work can be employed for any other wavelength in the VIS or IR.

With reference to the VAN and HAN states, the objective is to minimize diffraction in one state and maximize it along certain diffraction orders in the complimentary state, so as to achieve switchable optical beam steering. The incident optical field is a plane wave propagating along the  $y$  and polarized along the  $x$  axis ( $p$  polarization), impinging from the substrate side of the grating, as shown in Fig. 1. Light polarized along the  $z$  axis ( $s$  polarization) senses no variation between the two LC states and thus shows no tuning possibility, since the homeotropic anchoring conditions lead to LC local molecular orientation exclusively in the  $x$ - $y$  plane. The profiles of Figs. 2 and 3 indicate a more uniform variation for the HAN state, where the LC director shows a small gradient with respect to the  $x$  axis. This implies that if the matching condition  $n_e = n_g$  is satisfied,  $n_g$  being the polymer index, the  $x$ -polarized incident light senses a refractive index profile with minimal modulation along the grating vector. This can be verified by inspecting the  $q_1(x, y)$  profiles of Figs. 2(d) and 3(d) and noticing that  $q_1$  is directly related to the  $\varepsilon_{xx}$  element of the optical dielectric tensor. The matching condition can be satisfied by proper selection of the LC and polymer materials, in the case here investigated by using a high-index photopatternable polymer [44].

This matching condition aims to optimize the nondiffracting performance of the HAN state. The next step is a parametric study with respect to the geometrical features of the grating, namely pitch, amplitude, and filling factor, the latter in the case of the triangular grating. For each set of parameters a full-wave simulation based on the finite-element method is employed for both LC states [36]. The transmitted field  $\mathbf{E}^t$  is calculated in the superstratum, at a constant  $y = y_0$  plane over the extent of a grating period. The  $x$  component of  $\mathbf{E}^t$  is expanded in a 1-D Floquet series according to

$$E_x^t(x, y = y_0) = \sum_m E_{x,m}^t e^{-j\beta_m y}, \quad (12)$$

where  $\beta_m = \beta_0 + 2\pi m/p_0$ ,  $\beta_0 = (2\pi n_g/\lambda_0) \sin(\theta_{\text{inc}})$  being the polymer wave number projection in the direction of periodicity ( $x$  axis) for the general case of oblique incidence at

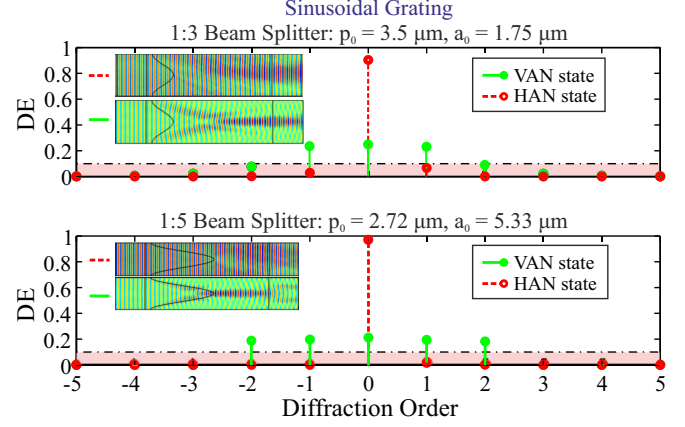


FIG. 4. (Color online) Diffraction efficiencies of the proposed sinusoidal bistable LC grating designed to split the transmitted optical power to three and five beams in the diffracting VAN state at  $\lambda = 633$  nm. Insets show the profile of the  $E_x$  component of the electric field.

an angle  $\theta_{\text{inc}}$ . The summation in Eq. (12) runs over diffracted modes that carry away optical power. This requires the condition that  $(2\pi n_g/\lambda_0)^2 > \beta_m^2$ , which ensures that the diffractive modes are propagating and not evanescent. The amplitudes  $E_{x,m}^t$  are obtained from orthogonality considerations with an integration over a grating period,

$$E_{x,m}^t = \frac{1}{p_0} \int_{y=y_0} E_x^t(x, y_0) e^{j\beta_m y} dx. \quad (13)$$

The diffraction efficiency for each diffraction mode is calculated by

$$DE_m = \frac{P_m}{P^i} = \frac{|E_{x,m}^t|^2}{|E_x^i|^2 |\cos \theta_m|}, \quad (14)$$

where  $P^i$ ,  $E_x^i$  are the power and amplitude of the incident electric field, respectively, and  $\cos \theta_m$  is given by

$$\cos \theta_m = \frac{\sqrt{(k_0 n_g)^2 - \beta_m^2}}{k_0 n_g}, \quad (15)$$

where  $k_0 = 2\pi/\lambda$  is the free-space wave number.

The parameter space of the geometrical features is scanned aiming at the following objectives: (a) the diffractive VAN state should split the incident optical beam into two, three, four, or five diffraction modes and (b) the diffraction efficiency of all undesired modes should be kept below 10% in both states. Figure 4 shows two examples based on the sinusoidal grating where three- and five-beam splitting is achieved. In the HAN state the grating shows very low  $x$ -dependent modulation of the refractive index and more than 90% of the total power remains in the nondiffracting ( $m = 0$ ) transmission mode. On the contrary, for the reported parameters the diffractive VAN state demonstrates splitting of the incident power in three and five beams with approximately equal efficiency, whereas all other modes remain suppressed below the 10% threshold.

The triangular grating provides an extra degree of freedom in the design, namely the filling factor  $f$ . This allows for additional capabilities compared to the sinusoidal grating, such as splitting in two or four beams, as demonstrated in the results

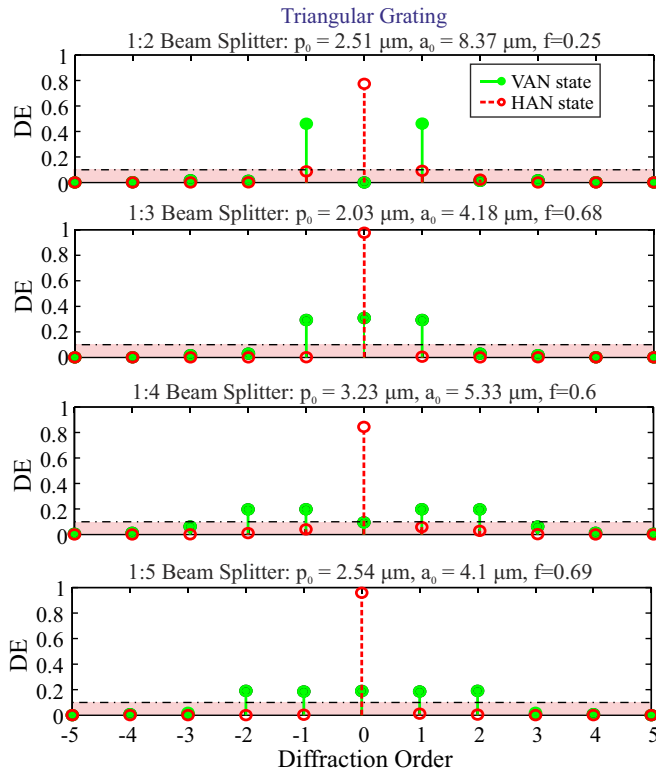


FIG. 5. (Color online) Diffraction efficiencies of the proposed triangular bistable LC grating designed to split the transmitted optical power to two, three, four, and five beams in the diffracting VAN state at  $\lambda = 633$  nm.

of Fig. 5, where the corresponding geometrical parameters for each scenario are reported. As commented in the LC profiles of Fig. 3, the LC profile of the HAN state is somehow less uniform compared to that of the sinusoidal grating, which can lead to higher efficiencies for the diffractive modes ( $m \neq 0$ ). Nevertheless, for the HAN state these still remain below the set threshold.

The results presented in Figs. 4 and 5 demonstrate the suitability of LC-ZB-DG for the design of switchable beam splitters. The critical condition is the refractive index matching between the LC extraordinary and the polymer indices at the target wavelength, which can be satisfied given the large variety of available nematic materials and polymers in the VIS or IR. Then, once the geometrical parameters have been optimized, the grating can be written using holographic, in the case of sinusoidal structures, or in general standard lithographic techniques such as those routinely employed in conventional display production lines [21]. The design procedure can be repeated for different wavelengths, provided the material indices are known. Finally, the same concept can be extended to other geometrical structures, such as blazed gratings, which are used to maximize the diffraction efficiency of a particular mode and achieve efficient beam steering [45,46].

Finally, preliminary investigations have shown that the performance of the proposed class of LC-ZB gratings is not dramatically sensitive to variations from the optimal geometrical parameters or material indices and wavelength

of operation, the latter demonstrated in Ref. [46] for the case of blazed LC-ZB beam steerers. This is attributed to the nonresonant nature of the optical diffraction phenomena, thus providing a degree of flexibility in terms of the fabrication of the optimized structures.

### C. Electro-optic switching in liquid-crystal zenithal bistable gratings: The dual-frequency case

The two stable states of the LC-ZB gratings correspond to local minima of the total LC bulk energy. These minima are separated by an energy barrier, which leads to bistability for a wide range of different grating geometries, even when one state has a lower energy. This barrier can be surpassed by applying a voltage that, depending on its amplitude, duration, and polarity, can cause defect nucleation or annihilation resulting in switching between the VAN and HAN states. The physics of this transition are governed by two separate effects, namely the dielectric and flexoelectric coupling of the nematic distortions with the applied electric field.

The dielectric effect causes the alignment of the LC molecules parallel (perpendicular) to the applied field in the case of positive (negative)  $\Delta\epsilon$  nematic materials. The flexoelectric effect stems from the large distortion of the director field near the grating surface in both states. When an electric field is applied perpendicular to the LC cell, a switching torque is produced, proportional to the flexoelectric polarization and the applied field, which causes defect annihilation or nucleation depending on the field polarity. This effect has been theoretically demonstrated for each one of the flexoelectric contributions associated with the coefficients  $p_1$  and  $p_2$  in Eq. (9) [38,39]. In practice, there is always a switching threshold, in general different for the two transitions, expressed in terms of the product  $\tau V_0$ , where  $\tau$  and  $V_0$  are the voltage pulse duration and amplitude, respectively [12,47,48]. Thus, the voltage threshold can be lowered by reducing the switching speed [12,49] and vice versa, depending on the application specifications. The pulse duration can be reduced to submillisecond times with voltages below 10 V, when using optimized LC mixtures, which provide high  $\Delta\epsilon$ , low viscosities, as well as an extended operative temperature range [50].

Another possibility for reversible switching is the use of dual-frequency LC materials, where the sign of  $\Delta\epsilon$  can be alternated by properly adjusting the frequency of the control voltage, typically in the range between 1 and 100 KHz. This driving technique relies on the dielectric effect, thus avoiding the complications of ionic migration that are associated in practice with flexoelectrically driven switching [49]. It is a standard option for the switching of LC-tunable devices, including bistable LC cells and gratings [20,51]. Here, we study a configuration for the one to five sinusoidal LC-ZB-DG beam splitter of Fig. 4, demonstrating efficient switching between the two states. A voltage is applied between the top LC-cell surface and below the polymer grating using two planar transparent ITO electrodes, as depicted in Fig. 6. It is remarked that the control electrodes are uniform and planar, thus facilitating the fabrication process compared to other electro-optically LC-based gratings, which typically employ specially patterned electrodes in order to achieve the required

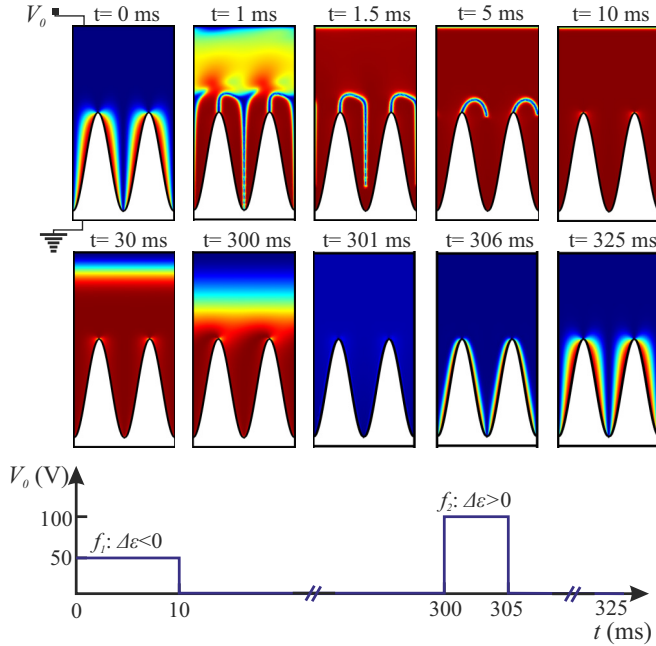


FIG. 6. (Color online) Switching between the HAN and VAN states for the one-to-five sinusoidal LC grating beam splitter of Fig. 4, for a dual-frequency nematic material. A rectangular pulse of amplitude  $V_0 = 50$  V and duration  $\tau_1 = 10$  ms applied at a high frequency where  $\Delta\epsilon < 0$  switches the grating from the VAN to HAN state. A second pulse with  $V_0 = 100$  V and  $\tau_2 = 5$  ms at a lower frequency such that  $\Delta\epsilon > 0$  switches the grating back to the VAN state.

voltage-tilt profiles. The distance between the bottom electrode and the grating’s trough is  $0.5 \mu\text{m}$ . The grating’s relative permittivity is equal to  $\epsilon_g = 4$ . The  $\mathbf{Q}$  tensor equations (11) are coupled consistently with Gauss’ law  $\nabla \cdot \mathbf{D} = 0$ , in order to calculate the spatial variation of both the LC orientation profile via  $q_i(x, y)$  and the electric field potential  $V(x, y)$ .

We consider that the device is initially in the VAN state. A rectangular pulse of  $\tau_1 = 10$  ms and  $V_0 = 50$  V is applied at  $t = 0$  with a frequency such that  $\Delta\epsilon < 0$ , using intentionally the material parameters of E7 so that the results are directly comparable with those of Figs. 2 and 4. We point out that this example only serves as a proof of concept of using dual-frequency LCs for the switching of the proposed gratings. Thus, there has been made no effort to optimize the grating’s response in terms of switching speed and voltage thresholds and material parameters. Owing to  $\Delta\epsilon < 0$ , the application of the electric field tilts the LC molecules along the grating vector, i.e., perpendicularly to the applied field. After 1 ms a pair of defects is formed, which then follow a filament-like trajectory towards the peak and trough of the grating. Such a behavior has also been observed both theoretically and experimentally in similar gratings with azimuthal bistability [20]. When the voltage is switched off, the LC molecules undergo an elastic relaxation that leads to the formation of the stable HAN state after approximately 300 ms. A pulse of  $\tau_2 = 5$  ms and  $V_0 = 100$  V is subsequently applied at a lower frequency such that  $\Delta\epsilon > 0$ . The LC molecules obtain an almost perpendicular alignment in less than 1 ms and relax to the VAN state within 20 ms after the pulse removal.

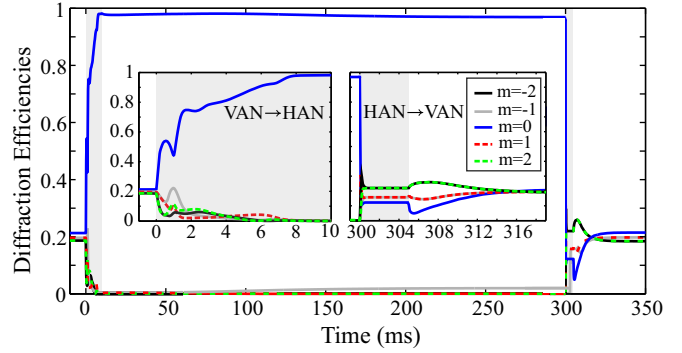


FIG. 7. (Color online) Temporal evolution of the diffraction efficiency for five diffraction orders ( $m = -2, -1, 0, 1, 2$ ) for the switching transition studied in Fig. 6. The grating’s optical diffractive properties remain unaffected by the nematic liquid crystal relaxation towards the HAN state after the removal of the VAN to HAN switching voltage.

These results indicate that in terms of the LC dynamics the overall switching speed is determined by the VAN to HAN transition. Nevertheless, contrary to display applications where the contrast between the dark and bright pixel state is the key parameter, the end property of the proposed LC-ZB-DG is the diffraction efficiency between the various modes. Figure 6 shows that after the removal of the VAN to HAN switching pulse, the LC index profiles shows no significant modulation along the  $x$  axis. This implies that during the transition to the HAN state, the grating remains mainly nondiffracting.

In order to assess the temporal dynamics of the grating efficiency we have calculated the diffraction efficiency for the five low-order modes, which are plotted in Fig. 7. It can be clearly observed that after the removal of the VAN to HAN switch pulse the structure remains highly nondiffracting with more than 90% of the total power remaining at the  $m = 0$  mode until the second pulse is applied. This general behavior was observed also for the other designs reported in Figs. 4 and 5. Therefore, as far as the optical diffraction properties of the LC-ZB-DG are concerned, the switching speed is limited by the HAN to VAN transition, which for the case studied is approximately 20 ms. The employment of efficient driving schemes, as discussed in the beginning of this section for the case of ZB displays, can optimize the proposed gratings in terms of switching speed and voltage requirements.

### III. CONCLUSIONS

In conclusion, this work has demonstrated that liquid-crystal zenithal-bistable gratings can be designed as tunable beam-splitting switches by optimizing their geometry and material selection. Conventional sinusoidal and triangular grating structures have been considered, showing that the latter offer more degrees of freedom that may provide extra functionalities. In both grating types, it has been demonstrated that the low-tilt HAN state shows very low diffraction, whereas the high-tilt VAN state can be adjusted to provide beam separation into two to five beams. A dielectric switching scheme based on dual-frequency LC has been investigated, revealing that the critical effect that determines the speed of the devices is

the HAN to VAN transition. These components leverage the ease of fabrication, stability, zero-power requirements, and addressing capabilities of zenithal bistable displays aiming at functional components that enable tunable light manipulation and steering for applications in the visible or infrared spectrum.

#### ACKNOWLEDGMENTS

This work was supported by the Italian Ministry of Foreign Affairs, Directorate General for the Country Promotion,

and by the European Union (European Social Fund, ESF) and Greek national funds through the Operational Program “Education and Lifelong Learning” of the National Strategic Reference Framework (NSRF) Research Funding Program THALES “Reinforcement of the interdisciplinary and/or inter-institutional research and innovation” (Project ANEMOS). The authors would also like to thank Dr. N. Mottram for helpful discussions and Dr. A. C. Tasolamprou for her contribution in the early stages of this work.

- 
- [1] D. C. Zografopoulos, R. Asquini, E. E. Kriezis, A. d’Alessandro, and R. Beccherelli, *Lab Chip* **12**, 3598 (2012).
- [2] J. Beeckman, K. Neyts, and P. J. M. Vanbrabant, *Opt. Eng.* **50**, 081202 (2011).
- [3] D. C. Zografopoulos and R. Beccherelli, *Plasmonics* **8**, 599 (2013).
- [4] A. C. Tasolamprou, B. Bellini, D. C. Zografopoulos, E. E. Kriezis, and R. Beccherelli, *J. Eur. Opt. Soc.-Rapid* **4**, 09017 (2009).
- [5] D. C. Zografopoulos, R. Beccherelli, A. C. Tasolamprou, and E. E. Kriezis, *Photon. Nanostruct.: Fundam. Appl.* **11**, 73 (2013).
- [6] D. C. Zografopoulos and R. Beccherelli, *Appl. Phys. Lett.* **102**, 101103 (2013).
- [7] P. F. McManamon, P. J. Bos, M. J. Escuti, J. Heikenfeld, S. Serati, H. Xie, and E. A. Watson, *Proc. IEEE* **97**, 1078 (2009).
- [8] P. Yeh and C. Gu, *Optics of Liquid Crystal Displays*, 2nd ed. (Wiley, New Jersey, 2010).
- [9] G. P. Bryan-Brown, C. V. Brown, and J. C. Jones, US Patent No. US6249332 (1995).
- [10] S. Kitson and A. Geisow, *Appl. Phys. Lett.* **80**, 3635 (2002).
- [11] L. A. Parry-Jones, E. G. Edwards, S. J. Elston, and C. V. Brown, *Appl. Phys. Lett.* **82**, 1476 (2003).
- [12] C. V. Brown, L. Parry-Jones, S. J. Elston, and S. J. Wilkins, *Mol. Cryst. Liq. Cryst.* **410**, 417 (2004).
- [13] C. Uche, S. J. Elston, and L. A. Parry-Jones, *J. Phys. D: Appl. Phys.* **38**, 2283 (2005).
- [14] C. Uche, S. J. Elston, and L. A. Parry-Jones, *Liq. Cryst.* **33**, 697 (2006).
- [15] C. Tsakonas, A. J. Davidson, C. V. Brown, and N. J. Mottram, *Appl. Phys. Lett.* **90**, 111913 (2007).
- [16] E. Willman, F. A. Fernández, R. James, and S. E. Day, *J. Display Technol.* **4**, 276 (2008).
- [17] S. Ladak, A. Davidson, C. V. Brown, and N. J. Mottram, *J. Phys. D: Appl. Phys.* **42**, 085114 (2009).
- [18] T. J. Spencer and C. M. Care, *Phys. Rev. E* **74**, 061708 (2006).
- [19] T. J. Spencer, C. M. Care, R. M. Amos, and J. C. Jones, *Phys. Rev. E* **82**, 021702 (2010).
- [20] A. J. Davidson, C. V. Brown, N. J. Mottram, S. Ladak, and C. R. Evans, *Phys. Rev. E* **81**, 051712 (2010).
- [21] C. Jones, in *Handbook of Visual Display Technology*, Vol. 3, edited by J. Chen *et al.* (Springer, Heidelberg, 2012), Chap. 7.3.5, pp. 1507–1543.
- [22] J. C. Jones, G. Bryan-Brown, E. Wood, A. Graham, P. Brett, and J. Hughes, *Proc. SPIE* **3955**, 84 (2000).
- [23] E. G. Edwards, C. V. Brown, E. E. Kriezis, S. J. Elston, S. C. Kitson, and C. J. P. Newton, *Mol. Cryst. Liq. Cryst.* **410**, 401 (2004).
- [24] J. Chen, P. J. Bos, H. Vithana, and D. L. Johnson, *Appl. Phys. Lett.* **67**, 2588 (1995).
- [25] J. Zhang, V. Ostroverkhov, K. D. Singer, V. Reshetnyak, and Yu. Reznikov, *Opt. Lett.* **25**, 414 (2000).
- [26] S. W. Kang, S. Sprunt, and L. C. Chien, *Appl. Phys. Lett.* **78**, 3782 (2001).
- [27] C. V. Brown, E. E. Kriezis, and S. J. Elston, *J. Appl. Phys.* **91**, 3495 (2002).
- [28] C. V. Brown and E. E. Kriezis, *Appl. Opt.* **42**, 2257 (2003).
- [29] G. P. Crawford, J. N. Eakin, M. D. Radcliffe, A. Callan-Jones, and R. A. Pelcovits, *J. Appl. Phys.* **98**, 123102 (2005).
- [30] C. Provenzano, P. Pagliusi, and G. Cipparrone, *Appl. Phys. Lett.* **89**, 121105 (2006).
- [31] J. Sun, A. K. Srivastava, L. Wang, V. G. Chigrinov, and H. S. Kwok, *Opt. Lett.* **38**, 2342 (2013).
- [32] L. De Sio, A. Veltri, C. Umeton, S. Serak, and N. Tabiryan, *Appl. Phys. Lett.* **93**, 181115 (2008).
- [33] D. E. Lucchetta, F. Vita, and F. Simoni, *Appl. Phys. Lett.* **97**, 231112 (2010).
- [34] L. De Sio, S. Serak, N. Tabiryan, and T. Bunning, *J. Mater. Chem. C* **2**, 3532 (2014).
- [35] G. Lombardo, H. Ayebe, and R. Barberi, *Phys. Rev. E* **77**, 051708 (2008).
- [36] Commercial finite-element solver “COMSOL Multiphysics” Ver. 4.4, Comsol Inc. (2014).
- [37] H. Yoshida, T. Matsui, A. Miura, N. Ikeda, M. Ochiai, Y. Sugimoto, H. Fujikawa, and M. Ozaki, *Opt. Mater. Express* **2**, 893 (2012).
- [38] L. A. Parry-Jones and S. J. Elston, *J. Appl. Phys.* **97**, 093515 (2005).
- [39] L. A. Parry-Jones, R. B. Meyer, and S. J. Elston, *J. Appl. Phys.* **106**, 014510 (2009).
- [40] J. F. Strömer, E. P. Raynes, and C. V. Brown, *Appl. Phys. Lett.* **88**, 051915 (2006).
- [41] Á. Buka and N. Éber (eds.), *Flexoelectricity in Liquid Crystals* (Imperial College Press, London, 2013).
- [42] H. Wang, T. X. Wu, S. Gauza, J. R. Wu, and S.-T. Wu, *Liq. Cryst.* **33**, 91 (2006).
- [43] J. Li, C.-H. Wen, S. Gauza, R. Lu, and S.-T. Wu, *J. Display Technol.* **1**, 51 (2005).
- [44] C. Lü, C. Guan, Y. Liu, Y. Cheng, and B. Yang, *Chem. Mater.* **17**, 2448 (2005).
- [45] C. Palmer, *Diffraction Grating Handbook* (Newport Corporation, New York, 2005).

- [46] D. C. Zografopoulos and E. E. Kriezis, *Opt. Lett.* **39**, 5842 (2014).
- [47] A. J. Davidson and N. J. Mottram, *Phys. Rev. E* **65**, 051710 (2002).
- [48] J. C. Jones and R. M. Amos, *Mol. Cryst. Liq. Cryst.* **543**, 57 (2011).
- [49] J. C. Jones, S. Beldon, P. Brett, M. Francis, and M. Goulding, *Proc. SID* **34**, 954 (2003).
- [50] M. Francis, M. J. Goulding, J. C. Jones, and S. Beldon, US Patent No. 2006/0115603 A1 (2006).
- [51] S. P. Palto and M. I. Barnik, *J. Exp. Theor. Phys.* **102**, 998 (2006).